GLAUCOMA

Measurement of macular ganglion cell layer and circumpapillary retinal nerve fiber layer to detect paracentral scotoma in early glaucoma

**Jeongmin Lee · Masanori Hangai · Yugo Kimura ·
Kohei Takayama · Changwon Kee ·
Nagahisa Yoshimura**

Abstract

Background Glaucoma patients with paracentral scotoma are at higher risk of losing central vision than those without glaucoma. The purpose of this study was to determine whether macular inner retinal layer (MIRL) measurements with spectral-domain optical coherence tomography (SD-OCT) outperform circumpapillary retinal nerve fiber layer (cpRNFL) measurements in discriminating between eyes with and without paracentral scotoma.

Methods This retrospective study included 63 early glaucomatous eyes of 63 patients with (PSI group) or without (PSF group) paracentral visual field (VF) defects. MIRL thicknesses, including macular ganglion cell complex (mGCC), macular ganglion cell layer + inner plexiform layer (mGCL+), macular RNFL (mRNFL), and cpRNFL thickness were measured using a SD-OCT instrument (3D OCT-2000). The MIRL and cpRNFL were divided into 50 grid cells and 36 sectors, respectively, which were numbered from center/temporal to periphery/nasal. Discriminating ability of the methods for number of cells/sectors with abnormal thickness (<5 % of normal) and average thickness in the hemisphere corresponding to the VF defects (termed hemi-thickness) was compared by area under the receiver operating characteristics curves (AROCs).

Results The number of abnormal nearest sectors of cpRNFL and all MIRL parameters were significantly smaller in the PSI group than in the PSF group ($P \leq 0.001$–0.047), whereas no significant differences were found for average or hemi-cpRNFL thickness. The AROCs of the number of abnormal nearest cells for mGCC and mGCL+ and average hemi-thickness for mGCC, mGCL+, and mRNFL were comparable and significantly higher than those of the number of abnormal nearest sectors/cells for cpRNFL ($P=0.0002$–0.0063) and mRNFL ($P=0.0003$–0.0267) parameters.

Conclusions Regional assessment of MIRL thickness as measured by SD-OCT may potentially be an effective method for predicting central involvement of VF defects in early glaucoma.

J. Lee · M. Hangai (✉) · Y. Kimura · K. Takayama · N. Yoshimura
Department of Ophthalmology and Visual Sciences, Kyoto
University Graduate School of Medicine, 54 Kawahara-cho,
Shogoin, Sakyo-ku, Kyoto 606-8507, Japan
e-mail: hangai@kuhp.kyoto-u.ac.jp

J. Lee
Yonsei Plus Eye Center, Bundang, Korea

C. Kee
Department of Ophthalmology, Samsung Medical Center,
Sungkyunkwan University School of Medicine, Seoul, Korea

Introduction

Glaucoma is an optic neuropathy characterized by the loss of cell bodies (somas) and axons of retinal ganglion cells (RGCs), resulting in the thinning of the ganglion cell layer (GCL) and the retinal nerve fiber layer (RNFL) [1–3]. Because the macular region contains more than 50 % of all the RGC somas [4], the loss of RGCs can be sensitively detected by measuring retinal thickness in the macular region [3, 5–15], and because all RGC axons gather to the optic disc, circumpapillary RNFL (cpRNFL) measured on a

circle scan centered at the optic disc is effective to detect global RGC loss. Recent studies have suggested that the macular inner retinal layer (MIRL) and cpRNFL thicknesses are comparable and complementary in discriminating between glaucomatous and normal eyes [10–15]. However, detection of macular RGC loss is expected to be advantageous for detecting structural changes associated with paracentral scotoma, although this remains to be proven.

Glaucomatous patients who have paracentral scotoma are at a greater risk of visual acuity loss [16] and decreased quality of vision in driving or reading [17, 18]. It is known that the center of the visual field, including the fixation, can be affected by glaucoma, even in early stages of the disease process [19–23]. It is suggested that patients with visual field defects that threaten fixation should be managed more aggressively because they have an increased risk of further loss of visual field close to fixation, which is in turn associated with loss of visual acuity [24]. Thus, it is of paramount importance to accurately assess paracentral glaucomatous damages. Currently, paracentral glaucomatous damages are detected as a visual field (VF) paracentral scotoma using standard automated perimetry (SAP) with the Humphrey Field Analyzer (HFA) and the Swedish Interactive Threshold Algorithm (SITA) 24-2 or 30-2 program (Carl Zeiss Meditec, Dublin, CA). The 24-2 or 30-2 test pattern has only 4 points within the central 4.2° in the radius of fixation, and 1 optional point within the fovea. Measurement of macular structures with optical coherence tomography (OCT) may be a quick and accurate alternative for screening to detect paracentral glaucomatous damages. However, the ability of the macular measurements to detect paracentral scotoma remains to be determined.

With the introduction of spectral-domain OCT (SD-OCT), a significant improvement in imaging resolution and speed was achieved, allowing segmentation of the macular inner retinal layers. The 3D-OCT-2000 (Topcon, Tokyo, Japan) is a commercially available SD-OCT device. With depth resolution of 6 μm in tissue and a scan speed of 50,000 A-scans per second, the 3D-OCT allows measurement of the combined or single thickness of the MIRL on a 3-dimensional (3D) raster scan data set [25]. The measurable layers include the macular ganglion cell complex (mGCC), which consists of three layers, the RNFL, GCL, and inner plexiform layer (IPL), and the macular ganglion cell layer + (mGCL+), which consists of two layers, the GCL and IPL, along with a single layer of the macular RNFL (mRNFL) [26, 27].

The purpose of the current study was to determine whether regional MIRL assessment can outperform regional cpRNFL measurement for detecting paracentral glaucomatous damages associated with paracentral scotoma in early glaucomatous patients. We classified patients into two VF groups according to the presence or absence of paracentral scotoma. We compared the ability to discriminate between the VF groups between MIRL and cpRNFL parameters assessed by 3D-OCT. We also sought to determine the best MIRL parameters to detect paracentral VF defects.

Materials and methods

Patients

The medical records from the database of patients who visited the glaucoma service and underwent 3D-OCT at Kyoto University Hospital from November 2010 to March 2012 were reviewed for inclusion into this retrospective study. Among them, glaucoma patients who had early VF defects as defined below were enrolled.

At an initial work-up, each patient had received a comprehensive ophthalmic examination, including measurement of refractive error and corneal radius by using an automated refractor/keratometer (ARK-530A, Nidek, Gamagori, Japan), measurement of best corrected visual acuity, axial length measurement by using partial laser interferometry (IOL master, Carl Zeiss Meditec, Dublin, CA), slit lamp examination, intraocular pressure measurements with a Goldmann applanation tonometer, gonioscopy, dilated fundoscopic examination, stereo disc photography (3-Dx simultaneous stereodisc camera; Nidek, Gamagori, Japan), red-free fundus photography (Heidelberg Retina Angiogram 2; Heidelberg Engineering, Heidelberg, Germany), standard automated perimetry (SAP) through the Humphrey Visual Field Analyzer with the 24-2 Swedish interactive threshold algorithm (24-2 SITA Standard; Carl Zeiss-Meditec, Dublin, CA), and the SD-OCT examination.

This study was approved by the Institutional Review Board and Ethics Committee of Kyoto University Graduate School of Medicine. All investigations adhered to the tenets of the Declaration of Helsinki. Informed consent was obtained from all of the patients in this study.

To be included the subjects had to have glaucoma with early VF defects as defined by MD>−6 dB [28], and normal and open angle by gonioscopy. A patient was diagnosed with glaucoma when there was a glaucomatous appearance of the optic disc, i.e., diffuse or localized neuroretinal rim thinning on stereoscopic color disc photographs, and/or RNFL defects with corresponding VF defects. Exclusion criteria were as follows: (1) best-corrected visual acuity worse than 20/40 (Snellen equivalent); (2) spherical equivalent refractive error of less than −6.00 diopter with spherical refraction within ±6.0 diopters and cylinder correction within ±3.0 diopters; (3) evidence of vitreoretinal disease, uveitis, nonglaucomatous optic neuropathy, diabetes mellitus, or any other systemic disease that might have affected the retina, optic nerve and visual field results, such as a cerebrovascular event, uncontrolled hypertension, and blood

disorders. When both eyes of a patient were eligible for this study, one eye was selected at random by using a coin-flip method.

Visual field testing and definition of visual field defects

Visual field defects resulting from glaucoma were defined by SAP with the 24-2 SITA Standard as (1) abnormal range on the glaucoma hemifield test or (2) the presence of at least three contiguous test points within the same hemifield on the pattern deviation probability plot at $P<0.05$, with at least 1 point at $P<0.01$, confirmed on two consecutive tests considered reliable based on fixation losses of 15 % or less, false-positive results of 15 % or less, and false-negative results of 15 % or less. The location and pattern of the defect had to be consistent between the two consecutive VF results. For glaucoma diagnosis, the two consecutive visual field tests were performed within 1 month of each other, and when the results of these did not agree, a third test was performed in another month.

Eyes with and without a paracentral VF defect were classified into two groups by using a modification of the definition provided in an earlier study [29]. Eyes were classified as paracentral-scotoma involved (PSI) group when glaucomatous VF defects were present in one hemifield within 10° of fixation, with at least 1 point at $P<0.01$ lying at the two innermost paracentral points, regardless of the presence of VF abnormality in the opposite hemifield. Eyes were classified as paracentral scotoma-free (PSF) group when glaucomatous VF defects were present in one hemifield without any point at $P<0.05$ or $P>0.01$ lying at the two innermost paracentral points. If both hemifields met either of these criteria, one hemifield was randomly enrolled for analysis.

Spectral domain OCT imaging and analysis

SD-OCT examinations were performed by using 3D-OCT 2000 within 1 month of the VF testing. This device uses a superluminescent diode laser with a center wavelength of 840 μm and a bandwidth of 50 nm as a light source. The acquisition rate of the device is up to 50,000 A-scans per second. The transverse and depth resolutions were ~20 and 6 μm, respectively. MIRL measurements were made with a macular 3D raster scan composed by 512×128 (vertical× horizontal) A-scans covering a cube of $7\times7\times2$ mm and centered on the fixation. cpRNFL measurements were made with a 3D raster scan centered at the optic disc composed by 512×128 (vertical × horizontal) A-scans covering a cube of $6\times6\times2$ mm and. To obtain more accurate lateral scan lengths during the measurement, the magnification effect in each eye was corrected according to the formula provided by the manufacturer (modified Littman's method), which is based on the refractive error, corneal radius, and axial length.

A well-trained examiner obtained the 3D-OCT data sets after pupillary dilatation with tropicamide 1 % and phenylephrine 2.5 %. The examiner discarded poor quality images with a signal strength score ("Q factor") <60, as recommended by the manufacturer, as well as any scans with visible eye motion or blinking artifacts (discontinuous jump), poor centration, or incorrect segmentation. The scans were repeated a maximum of three times when acceptable images were not obtained, and the eyes that had no acceptable images were excluded.

The boundaries of anatomical layers were determined by the built-in software (version 8.00) using a previously validated automated segmentation algorithm [26]. The MIRL analysis software automatically detects the foveal center of the macular cube, and selects a 6×6 mm region with its center at the foveal center. To assess regional abnormalities of MIRL thickness, the software divides the macular square into a 6×6 grid with 100 cells of 0.6×0.6 mm (Fig. 1a). Average regional thickness of mGCC, mGCL+, and mRNFL in each cell is calculated and compared to the normative database of the device. A cell is colored red when the average MIRL thickness within it is less than 1 % or yellow when the average MIRL thickness is between 1 % and 5 %, compared to the confidence intervals of the normative database (Fig. 2c–e, h–j).

In the present study, we numbered the 50 cells from 1 to 15 according to increasing distance from the fovea (Fig. 1a). The cells that were located at an identical distance from the foveal center were given the same number by referring to the concentric circles. We assigned the number 1 to the four innermost cells, and the farther from the fovea the cells were, the larger number we successively assigned as shown in Fig. 1a. We used the number and position of the cells with abnormal MIRL thickness for analysis. If there were no cells with abnormal MIRL thickness within the macular grid area, we assigned it the number 16. Each number included reciprocal regions from either hemifield (Fig. 1a).

For cpRNFL thickness measurements, the 3D OCT-2000 software automatically detects the center of the optic disc and places a calculation circle of approximately 3.4 mm diameter consisting of 1,024 A-scans around it. The cpRNFL thickness was measured as a distance between the anterior and posterior boundaries of the RNFL delineated by the computer algorithm. To assess regional abnormality of cpRNFL thickness, the 3D OCT-2000 software provides a significance map with 36 equal part sectors (Fig. 1b), with the temporal position designated number 1 and the nasal position number 19. Thus, the assigned numbers increase from the temporal position towards the nasal position, either in a clockwise or counter-clockwise direction (Fig. 1b). Abnormal cpRNFL thickness in each cpRNFL sector is displayed as a red color (<1 %) or yellow (≥1 % and <5 %) compared to the confidence intervals of the normative database (Fig. 2b, g).

The smallest number of cells and sectors with abnormal thickness in each eye should indicate the structural damages

Fig. 1 A schematic drawing of the numbering method to detect structural damages nearest the fovea in the MIRL and cpRNFL analyses. **a** We numbered the 50 cells from 1 to 15 according to increasing distance from the foveal center in MIRL significance map as shown in the schema; the cells that were located at an identical distance from the central foveal center were given the same number by referring to the concentric circles. **b** In the cpRNFL significance map with 36 sectors with equal angles, we designated the temporal position number 1 and the nasal position the number 19. The assigned numbers increased as they were away from the temporal position and towards the nasal position, either in the clockwise or counter-clockwise direction
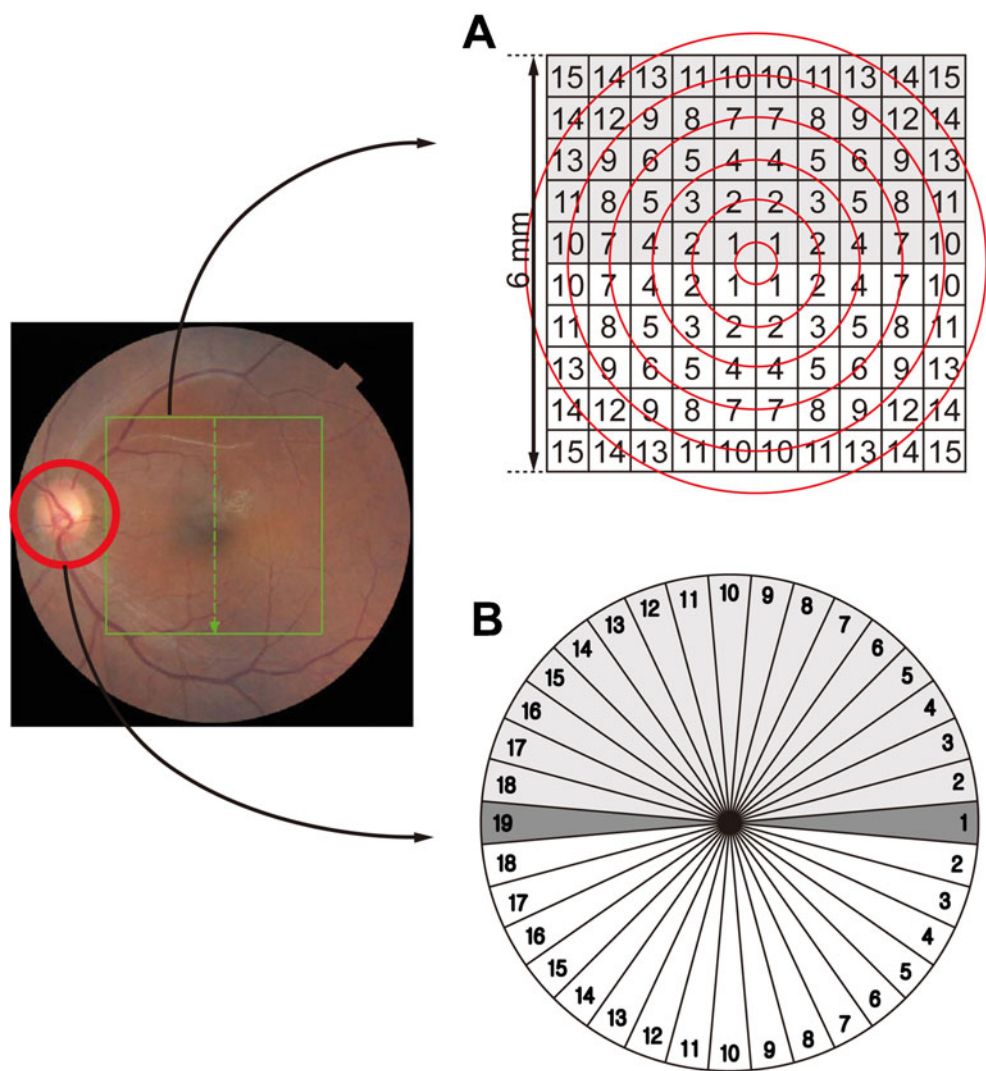
nearest to the fovea in MIRL and cpRNFL analyses, respectively. We used the low-numbered cells and sectors as structural parameters to detect paracentral scotoma in MIRL and cpRNFL analyses.

The average MIRL and cpRNFL thicknesses and average MIRL and cpRNFL thickness in the hemisphere corresponding to the VF defects used to classify the study eyes (termed hemi-thickness) were also used as structural parameters to detect paracentral scotoma.

Statistical analysis

The differences of categorical data between groups were evaluated using Chi-square test, and those of numerical data using a Mann–Whitney test. Spearman's correlation coefficients were calculated to determine associations between parameters. The area under the receiver operating characteristics curve (AROC) was calculated to assess the ability of each testing parameter to differentiate between two groups. Statistical analysis was done with SPSS for Windows

(version 12.0.0; SPSS, Chicago, Illinois). Commercially available software (MedCalc version 9.3.8.0, MedCalc Software, Mariakerke, Belgium) was used to compare the AROCs based on the method of DeLong et al [30]. A P-value<0.05 was considered statistically significant.

Results

After the exclusion of nine eyes that had no acceptable images, this retrospective study included 63 early glaucomatous eyes of 63 patients with (33 eyes of 33 patients, PSI group) or without (30 eyes of 30 patients, PSF group) paracentral VF defects. No significant differences were found in age (49.6±12.3 years vs. 55.5±11.2 years; $P=0.079$), gender (33.3 % vs. 46.7 % male, $P=0.280$), refractive error (-3.41 ± 1.99 diopter vs. -2.81 ± 1.58 diopter, $P=0.820$), mean deviation (-2.48 ± 2.27 dB vs. -2.29 ± 2.24 dB, $P=0.150$), or pattern standard deviation (5.74±2.75 dB vs. 5.20±2.60 dB; $P=0.429$) between the PSI and PSF groups, respectively
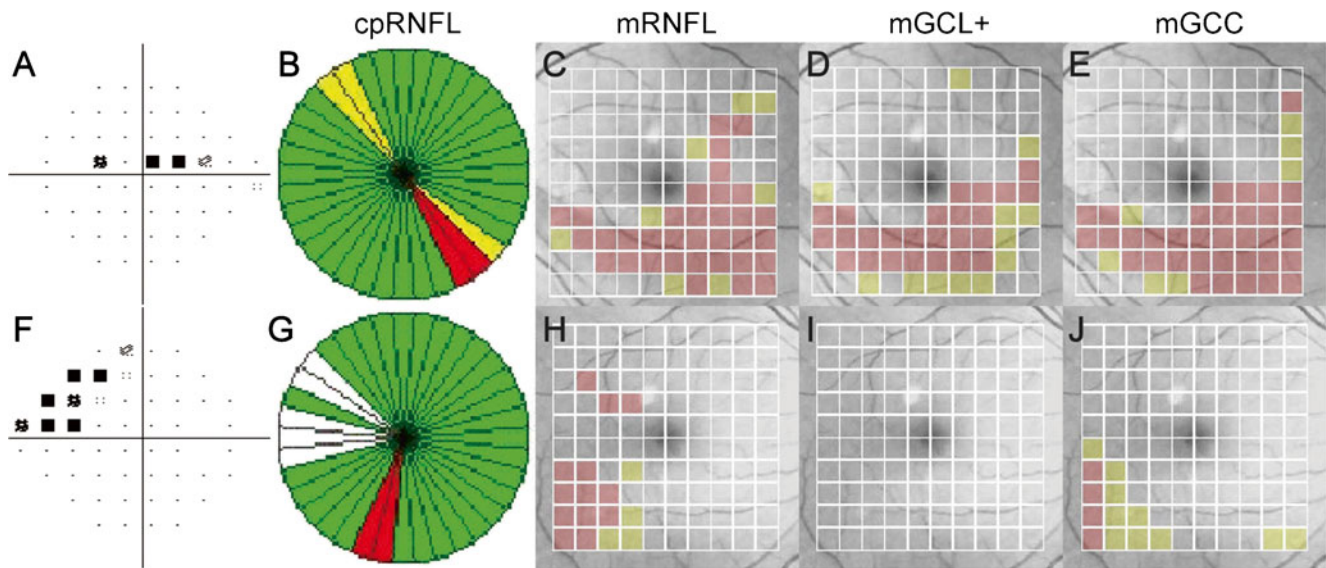
Fig. 2 Pattern deviation maps (**a** and **f**) of SAP24-2 and significance maps for cpRNFL (**b** and **g**), mRNFL (**c** and **h**), GCL+ (**d** and **i**), and GCC (**e** and **j**) in eyes with (**a**–**e**) and without (**f**–**j**) paracentral scotoma. **a** Left eye; **b** Right eye. *Red* and *yellow* colors indicate the abnormal (<1 %) and borderline (5 %) thinning of each parameter in each sector or cell, respectively, compared to confidence interval of the instrument normative database. The number of nearest abnormal cells was 2 for mRNFL, mGCL+, and mGCC in the eye with paracentral scotoma (**c**–**e**), whereas it was 3, 10, and 6, respectively, in the eye without paracentral scotoma (**h**–**j**). The number of nearest abnormal sectors for cpRNFL was 6 in the eye with paracentral scotoma (**b**), and 7 in the eye without paracentral scotoma (**g**). Thus, the locations of abnormal cells for mRNFL, mGCL+, and mGCC were much closer to the foveal center in eyes with paracentral scotoma, whereas those of abnormal sectors for cpRNFL were not largely different

(Table 1). The glaucomatous eyes in this study included 23 eyes with high-tension, open-angle glaucoma (known untreated IOP>21 mmHg for two measurements; PSI, 12 eyes; and PSF, 11 eyes) and 40 eyes with normal-tension, open-angle glaucoma (untreated IOP≤21 mmHg at all times; PSI, 21 eyes; and PSF, 19 eyes). The distribution of PSI and PSF was not significantly different between groups ($P=0.29$).

MIRL and cpRNFL parameters measured with 3D-OCT for each group are shown in Table 2. No significant differences were found in mean signal strength score for macular scan (74.5±7.9 in PSI group and 74.9±8.6 in PSF group;

$P=0.86$) or for cpRNFL scan (73.4±6.3 in PSI group and 75.0±7.6 in PSF group; $P=0.95$) between groups.

Among cpRNFL parameters, the number of abnormal nearest sectors was significantly smaller in the PSI group than in the PSF group ($P=0.047$), whereas no significant differences were found for average or hemi-cpRNFL thickness ($P=0.440$ and 0.083; Table 2). Therefore, only the number of abnormal nearest sectors was used as a cpRNFL parameter for AROC comparison.

By contrast, all of the MIRL parameters were significantly different between groups. The number of abnormal nearest

Fig. 3 ROC curves for MIRL and cpRNFL parameters. **a** The number of nearest abnormal sectors/cells. **b** Average hemi-MIRL thicknesses
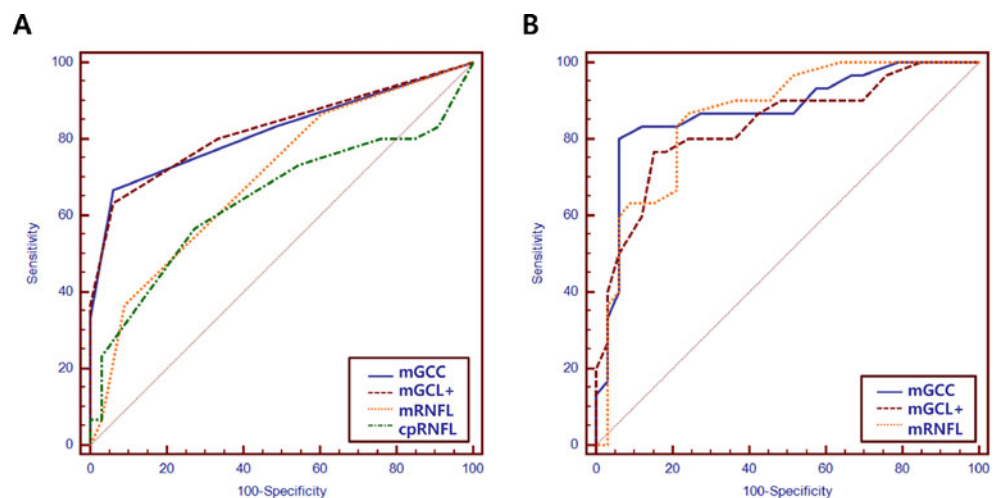
Table 1 Comparison of demographics between groups

Variables	PSI group	PSF group	P value
Age (years)	49.6±12.3	55.5±11.2	0.079[a]
MD (dB)	−2.48±2.27	−2.29±2.24	0.150[a]
PSD (dB)	5.74±2.75	5.20±2.60	0.429[a]
Right, n (%)	17 (51.5)	15 (50.0)	0.904[b]
Male, n (%)	11 (33.3)	14 (46.7)	0.280[b]
Refraction (D)	−3.41±1.99	−2.81±1.58	0.820[a]

Decimals data are mean ± standard deviation

D diopter; *MD* mean deviation; *PSD* pattern standard deviation; *PSI* paracentral scotoma involving; *PSF* paracentral scotoma free

[a] Mann-Whitney U test

[b] Chi-square test

The cpRNFL, mGCC, mGCL+, and mRNFL all showed significant positive correlations between the number of nearest abnormal sectors/cells and average thickness, but the correlation coefficients were poor or fair (P=0.030–<0.001, rho= 0.274–0.688, Table 3). The mGCC, mGCL+, and mRNFL showed significant positive correlations between the number of the nearest abnormal cells and average hemi-thickness (P< 0.001), but the cpRNFL did not (Table 3). The correlation coefficients were good or moderate for mGCC (rho=0.807) and mGCC+ (rho=0.717).

The AROCs to discriminate between groups were worst in the number of abnormal nearest sectors of cpRNFL (0.644) (Table 2 and Fig. 3). The AROCs of all the average MIRL thickness parameters were moderate (0.706–0.770). The number of abnormal nearest cells for mGCC and mGCL+ and average hemi-thickness for mGCC, mGCL+, and mRNFL showed fair to good AROCs (Table 2). The AROCs of the number of abnormal nearest cells of mGCC and mGCL+ and average hemi-thickness for mGCC, mGCL+, and mRNFL were comparable (Table 4 and Fig. 3). The number of abnormal nearest cells of mGCC

cells in all of the MIRL measurements was significantly smaller in the PSI group than in the PSF group (mGCC, P< 0.001; mGCL+, P<0.001; mRNFL, P=0.001, Table 2). The average and hemi-MIRL thicknesses were significantly smaller in PSI group than in the PSF group (P≤0.001–0.005).

Table 2 Thickness parameters measured with SD-OCT and area under the receiver-operating characteristic curves for comparison between the two groups

Variables	PSI group	PSF group	P value[a]	AROC	95 % CI
cpRNFL scan					
Signal strength	73.4±6.3	75.0±7.6	0.276		
Number of abnormal nearest sectors	4.5±1.9	5.5±2.7	**0.047**	0.644	0.463 – 0.825
Average thickness (μm)	83.33±11.05	80.57±11.76	0.440	–	0.300 – 0.587
Average hemi-cpRNFL thickness (μm)[b]	90.94±15.06	82.47±19.06	0.083	–	0.231 – 0.515
Macular scan for MIRL parameters					
Signal strength	74.5±7.9	74.9±8.6	0.907		
Number of abnormal nearest cells					
mGCC	1.5±0.6	4.1±3.2	**<0.001**	0.821	0.711 – 0.931
mGCL+	1.4±0.6	4.6±4.2	**<0.001**	0.826	0.718 – 0.933
mRNFL	1.7±0.7	2.6±1.5	**0.001**	0.718	0.592 – 0.844
Average thickness (μm)					
mGCC	82.45±8.71	91.53±9.21	**<0.001**	0.770	0.653 – 0.886
mGCL+	58.21±5.73	62.6±5.18	**0.005**	0.706	0.577 – 0.834
mRNFL	24.36±4.47	28.90±4.78	**<0.001**	0.763	0.644 – 0.882
Average hemi-thickness (μm)[b]					
mGCC	71.67±9.79	87.90±10.74	**<0.001**	0.874	0.781 – 0.967
mGCL+	53.67±5.01	61.37±6.05	**<0.001**	0.835	0.733 – 0.937
mRNFL	18.55±5.78	26.43±5.14	**<0.001**	0.862	0.770 – 0.954

The values written in bold means statistically significant

Decimals data are mean ± standard deviation

AROC area under the receiver-operating characteristic (ROC) curves; *mGCC* macular ganglion cell complex; *cpRNFL* circumpapillary retinal nerve fiber layer; *mGCL+* macular ganglion cell layer + inner plexiforma layer; *MIRL* macular inner retinal layer; *mRNFL* macular retinal nerve fiber layer; *PSI* paracentral scotoma involving; *PSF* paracentral scotoma free

[a] Mann-Whitney U test

[b] Average thickness in the hemisphere corresponding to the visual field defects classified to PSI or PSF

Table 3 Spearman's correlation coefficients between the number of nearest abnormal sectors/cells and thickness parameters

Variables		Average thickness		Average hemi-thickness	
		P	Correlation coefficients	P	Correlation coefficients
Number of Nearest abnormal sectors/cells	cpRNFL	**0.030**	**0.274**	0.433	−0.101
	mGCC	**<0.001**	**0.688**	**<0.001**	**0.807**
	mGCL+	**<0.001**	**0.561**	**<0.001**	**0.717**
	mRNFL	**<0.001**	**0.532**	**<0.001**	**0.599**

The values written in bold means statistically significant

mGCC macular ganglion cell complex; *cpRNFL* circumpapillary retinal nerve fiber layer; *mGCL+* macular ganglion cell layer + inner plexiforma layer; *mRNFL* macular retinal nerve fiber layer

and mGCL+ and average hemi-thickness for mGCC, mGCL+, and mRNFL showed significantly higher AROCs than the number of abnormal nearest sectors/cells of the cpRNFL parameter (P=0.0002–0.0063), and of the mRNFL parameter (P=0.0003–0.0267) (Table 4).

Discussion

Following the study by Zeimer et al. [31] that indicated the usefulness of macular thickness measurements as an indicator of glaucomatous damages, many studies have tested the ability of macular retinal and retinal layer structures as measured with various OCT instruments to discriminate between normal and glaucomatous eyes [5–15, 31]. However, to our knowledge, no studies have been available regarding the ability of OCT parameters to distinguish between eyes with and without paracentral scotoma. The current study suggested that regional structural assessment of macular inner retinal layers, such as mGCC, mGCL+, and mRNFL is a better indicator of paracentral scotoma than cpRNFL measurement. Although average MIRL thickness is reportedly comparable in glaucoma discriminating ability with average cpRNFL thickness [10–15], MIRL parameters appear to outperform cpRNFL parameters in detecting paracentral scotoma in glaucoma.

Theoretically, when the RGC somas are closer to the fovea, the axons from the RGCs that pass the cpRNFL circle are closer to the line passing the foveal and disc centers. Furthermore, regional cpRNFL thickness in the temporal sectors should also reflect RGC loss near the fovea. Regardless of this, MIRL parameters had significantly better ability than cpRNFL parameters for detecting paracentral damages. Differences in anatomy at the cellular level that constitute the GCL and RNFL may account for these results. The RGC axons running through each cpRNFL sector come from RGC cell bodies that exist in the wider area. Therefore, even if the RNFL in a sector includes RGC axons originating from RGC somas near the fovea, it also includes RGC axons originating from the RGC somas located further from the fovea. This variation in the locations of the RGC somas that constitute the RNFL in each sector may be responsible for the lesser ability of regional cpRNFL to detect paracentral damages. By contrast, because mGCC and mGCL+ thicknesses in each grid cell reflect the number of RGC somas located exactly within the cell, these parameters in each cell are able to detect the loss of RGCs limited to that cell.

In the present study, the lowest number of abnormal mRNFL cells was inferior to the lowest abnormal cell numbers in the mGCC and mGCL+ as an indicator of paracentral scotoma. As mentioned above, the abnormal thickness of mRNFL in certain cells does not necessarily represent damages to the RGC soma within the cells, because a large portion of the RGC axons running through each cell area originate from RGC soma that exist in more peripheral locations. In addition, anatomically, the GCL thickness is greatest roughly 1 mm from the foveal center [4, 27, 32–34] that favors a large dynamic range of the GCL measurement in the parafoveal region. In contrast, the mRNFL is thinnest near the fovea and increases in thickness as a function of the distance from the foveal center in normal eyes [27, 33, 34]. The difference in dynamic range for measurements in the parafoveal region may possibly account for our finding that regional mRNFL assessment is a relatively poor indicator of paracentral scotoma.

In the current study, the locations of abnormal MIRL thicknesses and the hemi-MIRL thicknesses were comparable in detecting paracentral scotoma. We did not expect this result, because hemi-MIRL thicknesses include the peripheral macula as well as the central macula. The damages to RGCs in the peripheral macula do not appear to cause paracentral VF damages. Among the innermost 12 test points of SAP24-2 corresponding to the macular scan area, the innermost four test points correspond to the mid- to central macular region with thick GCL, whereas the other 8 points correspond to the peripheral macular region with the thinnest GCL in the macula [4, 27, 32–34]. Thus, VF sensitivity loss in the innermost 4 points results from damages to the mid- to paracentral macular GCL. The lower the number of abnormal MIRL cells, the greater the area of the

Table 4 Comparison of area under the receiver operating characteristics curve

Variables		Nearest Abnormal Sectors or Cells				Average thickness			Average hemi-thickness		
		cpRNFL	mGCC	mGCL+	mRNFL	mGCC	mGCL+	mRNFL	mGCC	mGCL+	mRNFL
Nearest abnormal sectors or cells	cpRNFL	–	**0.0039**	**0.0063**	0.3165	**0.0465**	0.3754	0.0870	**0.0002**	**0.0009**	**0.0013**
	mGCC		–	0.8484	**0.0267**	0.3094	0.0591	0.2733	0.1398	0.7454	0.3553
	mGCL+			–	**0.0216**	0.2870	0.0593	0.2495	0.1973	0.8433	0.3995
	mRNFL				–	0.3749	0.8643	0.4483	**0.0003**	**0.0191**	**0.0057**
Average thickness	mGCC					–	0.0578	0.8489	**0.0164**	0.1270	0.0789
	mGCL+						–	0.3583	**0.0045**	**0.0034**	**0.0278**
	mRNFL							–	**0.0123**	0.2093	**0.0184**
Average hemi-thickness[a]	mGCC								–	0.1999	0.6858
	mGCL+									–	0.5906
	mRNFL										–

The values written in bold means statistically significant

Each number means a P-value for comparison between two parameters.

Comparison was performed using the method of DeLong et al. [30]

[a] Average thickness in the hemisphere corresponding to the visual field defects classified to PSI or PSF

mid- to paracentral macula that is expected to be involved in glaucomatous damages. In the current study, considerable correlations were found between the number of nearest abnormal cells for mGCC and mGCL+ and their hemiretinal thicknesses, but correlation between the number of nearest abnormal cells for mRNFL and its hemiretinal thickness was less. This is probably because the GCL is thick and the RNFL is thin in the mid- to paracentral macula [4, 27, 32–34]. Thus, involvement of the mid to central macular GCL in glaucomatous damages appears to correlate well with more severe hemiretinal MIRL thinning.

Average MIRL thicknesses were inferior to the average hemi-MIRL thicknesses as an indicator of paracentral scotoma. Average MIRL thicknesses include the contralateral hemisphere that was not associated with the VF defects concerned, which may have a diluting effect on the result. Thus, measurement of MIRL thickness limited to the hemisphere associated with the VF defects concerned may have improved the ability to discriminate between PSI and PSF groups.

A possible limitation of the current study is the use of only Japanese participants. It is known that MIRL and cpRNFL thicknesses differ with ethnicity [35, 36]. However, the anatomical characteristics of the RNFL and GCL we discussed above should be common among all humans. Therefore, the results of this study are expected to hold true for other ethnic groups, although this remains to be determined. A second possible limitation would be that the current study is a cross-sectional study, and not a longitudinal study. The study patients were beforehand classified into two groups according to whether they had paracentral scotoma. To confirm that the regional assessment of MIRL thicknesses is predictive for the development of paracentral scotoma, prospective longitudinal studies are needed in the future. A third limitation of this study is that we used SAP24-2 to define paracentral scotoma because of the retrospective nature of the study. Paracentral VF defects are represented only by the innermost four test points in the 24-2 program, which tests an area of 24° around the fixation. Because the resolution capacity of this program is insufficient to recognize paracentral VF defects (approximately 6° between each test point), the use of SAP10-2 (10° around the fixation with a resolution of approximately 2° between each test point) would be more appropriate. We plan to perform a prospective study using SAP10-2 to confirm the present results. A fourth limitation is that the reproducibility and variability of the SD-OCT device used to measure cpRNFL are not the highest of the commonly used SD-OCT devices [34]. The performance of the built-in software algorithm to measure cpRNFL thickness may affect the results.

In conclusion, the results of the current study suggest that the regional assessment of MIRL thicknesses is a better indicator of paracentral scotoma than that of cpRNFL parameters. It is important for clinicians to be aware of central involvement of VF defects in early glaucoma. A quick and simple screening method is desirable for this purpose. Highlighting the distance of abnormal cells from the fovea is an easy way to evaluate the proximity of structural abnormalities to the fovea at a glance. Clinically, it would be more useful to be able to indicate the location (nasal versus temporal, superior versus inferior) of the paracentral scotoma, which we plan to investigate in a large-scale study. Regional assessment of MIRL thicknesses may potentially be useful for the management of glaucoma in order to prevent progressive central vision loss.

References

1. Quigley HA, Dunkelberger GR, Green WR (1989) Retinal ganglion cell atrophy correlated with automated perimetry in human eyes with glaucoma. Am J Ophthalmol 107:453–464

2. Quigley HA, Miller NR, George T (1980) Clinical evaluation of nerve fiber layer atrophy as an indicator of glaucomatous optic nerve damage. Arch Ophthalmol 98:1564–1571

3. Medeiros FA, Zangwill LM, Bowd C, Vessani RM, Susanna R Jr, Weinreb RN (2005) Evaluation of retinal nerve fiber layer, optic nerve head, and macular thickness measurements for glaucoma detection using optical coherence tomography. Am J Ophthalmol 139:44–55

4. Curcio CA, Allen KA (1990) Topography of ganglion cells in human retina. J Comp Neurol 300:5–25

5. Greenfield DS, Bagga H, Knighton RW (2003) Macular thickness changes in glaucomatous optic neuropathy detected using optical coherence tomography. Arch Ophthalmol 121:41–46

6. Wollstein G, Schuman JS, Price LL, Aydin A, Beaton SA, Stark PC, Fujimoto JG, Ishikawa H (2004) Optical coherence tomography (OCT) macular and peripapillary retinal nerve fiber layer measurements and automated visual fields. Am J Ophthalmol 138:218–225

7. Leung CK, Chan WM, Yung WH, Ng AC, Woo J, Tsang MK, Tse RK (2005) Comparison of macular and peripapillary measurements for the detection of glaucoma: an optical coherence tomography study. Ophthalmology 112:391–400

8. Wollstein G, Ishikawa H, Wang J, Beaton SA, Schuman JS (2005) Comparison of three optical coherence tomography scanning areas for detection of glaucomatous damage. Am J Ophthalmol 139:39–43

9. Ojima T, Tanabe T, Hangai M, Yu S, Morishita S, Yoshimura N (2007) Measurement of retinal nerve fiber layer thickness and macular volume for glaucoma detection using optical coherence tomography. Jpn J Ophthalmol 51:197–203

10. Ishikawa H, Stein DM, Wollstein G, Beaton S, Fujimoto JG, Schuman JS (2005) Macular segmentation with optical coherence tomography. Invest Ophthalmol Vis Sci 46:2012–2017

11. Tan O, Li G, Lu AT, Varma R, Huang D (2008) Mapping of macular substructures with optical coherence tomography for glaucoma diagnosis. Ophthalmology 115:949–956

12. Tan O, Chopra V, Lu AT, Schuman JS, Ishikawa H, Wollstein G, Varma R, Huang D (2009) Detection of macular ganglion cell loss in glaucoma by Fourier-domain optical coherence tomography. Ophthalmology 116:2305–2314

13. Seong M, Sung KR, Choi EH, Kang SY, Cho JW, Um TW, Kim YJ, Park SB, Hong HE, Kook MS (2010) Macular and peripapillary retinal nerve fiber layer measurements by spectral domain optical coherence tomography in normal-tension glaucoma. Invest Ophthalmol Vis Sci 51:1446–1452

14. Nakatani Y, Higashide T, Ohkubo S, Takeda H, Sugiyama K (2011) Evaluation of macular thickness and peripapillary retinal nerve fiber layer thickness for detection of early glaucoma using spectral domain optical coherence tomography. J Glaucoma 20:252–259

15. Kim NR, Lee ES, Seong GJ, Kim JH, An HG, Kim CY (2010) Structure-function relationship and diagnostic value of macular ganglion cell complex measurement using Fourier-domain OCT in glaucoma. Invest Ophthalmol Vis Sci 51:4646–4651

16. Kolker AE (1977) Visual prognosis in advanced glaucoma: a comparison of medical and surgical therapy for retention of vision in 101 eyes with advanced glaucoma. Trans Am Ophthalmol Soc 75:539–555

17. Coeckelbergh TR, Brouwer WH, Cornelissen FW, Van Wolffelaar P, Kooijman AC (2002) The effect of visual field defects on driving performance: a driving simulator study. Arch Ophthalmol 120:1509–1516

18. Fujita K, Yasuda N, Oda K, Yuzawa M (2006) [Reading performance in patients with central visual field disturbance due to glaucoma]. Nihon Ganka Gakkai Zasshi 110:914–918

19. Stamper RL (1984) The effect of glaucoma on central visual function. Trans Am Ophthalmol Soc 82:792–826

20. Anctil JL, Anderson DR (1984) Early foveal involvement and generalized depression of the visual field in glaucoma. Arch Ophthalmol 102:363–370

21. Koseki N, Araie M, Yamagami J, Suzuki Y (1995) Sectorization of central 10-deg visual field in open-angle glaucoma. An approach for its brief evaluation. Graefes Arch Clin Exp Ophthalmol 233:621–626

22. Schiefer U, Papageorgiou E, Sample PA, Pascual JP, Selig B, Krapp E, Paetzold J (2010) Spatial pattern of glaucomatous visual field loss obtained with regionally condensed stimulus arrangements. Invest Ophthalmol Vis Sci 51:5685–5689

23. Sihota R, Gupta V, Tuli D, Sharma A, Sony P, Srinivasan G (2007) Classifying patterns of localized glaucomatous visual field defects on automated perimetry. J Glaucoma 16:146–152

24. Membrey WL, Poinoosawmy DP, Bunce C, Fitzke FW, Hitchings RA (2000) Comparison of visual field progression in patients with normal pressure glaucoma between eyes with and without visual field loss that threatens fixation. Br J Ophthalmol 84:1154–1158

25. Pierro L, Gagliardi M, Iuliano L, Ambrosi A, Bandello F (2012) Retinal nerve fiber layer thickness reproducibility using seven different OCT instruments. Invest Ophthalmol Vis Sci 53:5912–5920

26. Yang Q, Reisman CA, Wang Z, Fukuma Y, Hangai M, Yoshimura N, Tomidokoro A, Araie M, Raza AS, Hood DC, Chan K (2010) Automated layer segmentation of macular OCT images using dual-scale gradient information. Opt Express 18:21293–21307

27. Ooto S, Hangai M, Tomidokoro A, Saito H, Araie M, Otani T, Kishi S, Matsushita K, Maeda N, Shirakashi M, Abe H, Ohkubo S, Sugiyama K, Iwase A, Yoshimura N (2011) Effects of age, sex, and axial length on the three-dimensional profile of normal macular layer structures. Invest Ophthalmol Vis Sci 52:8769–8779

28. Hodapp E, Parrish RK II, Anderson DR (1993) Clinical decisions in glaucoma. Mosby-Year Book, St Louis

29. Park SC, De Moraes CG, Teng CC, Tello C, Liebmann JM, Ritch R (2011) Initial parafoveal versus peripheral scotomas in glaucoma: risk factors and visual field characteristics. Ophthalmology 118:1782–1789

30. DeLong ER, DeLong DM, Clarke-Pearson DL (1988) Comparing the areas under two or more correlated receiver operating characteristic curves: a nonparametric approach. Biometrics 44:837–845

31. Zeimer R, Asrani S, Zou S, Quigley H, Jampel H (1998) Quantitative detection of glaucomatous damage at the posterior pole by retinal thickness mapping. A pilot study. Ophthalmology 105:224–231

32. Wang M, Hood DC, Cho JS, Ghadiali Q, De Moraes CG, Zhang X, Ritch R, Liebmann JM (2009) Measurement of local retinal ganglion cell layer thickness in patients with glaucoma using frequency-domain optical coherence tomography. Arch Ophthalmol 127:875–881

33. Nakano N, Hangai M, Nakanishi H, Mori S, Nukada M, Kotera Y, Ikeda HO, Nakamura H, Nonaka A, Yoshimura N (2011) Macular ganglion cell layer imaging in preperimetric glaucoma with speckle noise-reduced spectral domain optical coherence tomography. Ophthalmology 118:2414–2426

34. Mwanza JC, Oakley JD, Budenz DL, Chang RT, Knight OJ, Feuer WJ (2011) Macular ganglion cell-inner plexiform layer: automated detection and thickness reproducibility with spectral domain-optical coherence tomography in glaucoma. Invest Ophthalmol Vis Sci 52:8323–8329

35. Knight OJ, Girkin CA, Budenz DL, Durbin MK, Feuer WJ (2012) Effect of race, age, and axial length on optic nerve head parameters and retinal nerve fiber layer thickness measured by Cirrus HD-OCT. Arch Ophthalmol 130:312–318

36. Girkin CA, McGwin G Jr, Sinai MJ, Sekhar GC, Fingeret M, Wollstein G, Varma R, Greenfield D, Liebmann J, Araie M, Tomita G, Maeda N, Garway-Heath DF (2011) Variation in optic nerve and macular structure with age and race with spectral-domain optical coherence tomography. Ophthalmology 118:2403–2408